Energy & Environmental Science

ROYAL SOCIETY OF CHEMISTRY

PAPER

View Article Online
View Journal | View Issue

Cite this: *Energy Environ. Sci.*, 2025, **18**, 9254

Investigating the effect of lithiation on polycrystalline NMC811 Li-ion battery cathode cracking using *in situ* SEM micromechanical testing

Aigerim Omirkhan, *[ab] Oriol Gavalda-Diaz, [a] Siyang Wang, [a] Ifan E. L. Stephens, [ab] Finn Giuliani [a] and Mary P. Ryan *[ab]

Received 18th February 2025,
Accepted 16th September 2025

DOI: 10.1039/d5ee00976f

rsc.li/ees

The mechanical degradation of polycrystalline NMC811 cathode particles during electrochemical cycling was investigated using *in situ* powder compression and nanoindentation. The research demonstrates a significant reduction in particle strength upon the first delithiation, with only partial recovery upon (re)lithiation. Continuous cycling within the normal operating window leads to further mechanical degradation, likely due to cracking and potential rock-salt layer formation. This method can be applied to other materials chemistries and used as a reliable and quick method to quantify the mechanical stability of other spherical particles exposed to electrochemical cycling.

Broader context

Despite the recent uptake of lithium iron phosphate cathode chemistry owing to decreased production costs, polycrystalline NMC811 cathode material remains and is predicted to stay in the EV cathode chemistry mix thanks to its high energy density. Despite the high capacity, the stability of lithium intercalation in polycrystalline NMC811 is average. Particle cracking, reported as one of the culprits for capacity reduction in these batteries, takes place due to the combination of electrochemical and mechanical interactions during charging. In this work we directly measure evolution of mechanical properties of NMC811 cathode material as a function of battery cycling using micromechanical testing *in situ* SEM. We show that the strength of the particles that make up the cathode dramatically decreases when lithium ions shuttle out of the cathode during charging. When the battery is discharged, we observe partial recovery of the mechanical strength. We also report that particles charged at slow rate are stronger thanks to sufficient time for Li diffusion. This method can be applied to other materials chemistries and used as a reliable and quick method to quantify the mechanical stability of other spherical particles exposed to electrochemical cycling, therefore being of great importance to the battery research community.

Introduction

Layered Ni-rich $LiNi_xMn_yCo_{1-x-y}O_2$ (NMC) cathode materials are becoming increasingly popular for the state-of-the-art electric vehicle electrodes due to their high storage capacities. The electronic configuration of nickel in $LiMO_2$ layered structures allows for greater lithium utilization because of reduced electron delocalization compared with that of cobalt.[1] Although the theoretical capacity of NMC materials is 275 mAh g^{-1}, the practical capacities are significantly lower owing to structural instabilities, including cracking, in highly delithiated states and the need for high voltages resulting from a sloped voltage profile during charging.[2] Nevertheless, at the same upper cut-off potential, $LiNi_{0.8}Mn_{0.1}Co_{0.1}O_2$ (NMC811) achieves a higher capacity compared to $LiNi_{0.33}Mn_{0.33}Co_{0.33}O_2$ (NMC111).[2]

The stability of lithium intercalation, or capacity retention, was found to be inversely proportional to the nickel content in the NMC layered cathodes.[3] Numerous studies have reported apparent reduction of capacity with the number of cycles in lithium-ion batteries (LIBs) utilising NMC811 polycrystalline cathodes.[4–6] Although capacity and power reduction are easily measurable, they do not identify the specific mechanism responsible for battery degradation. Edge *et al.*[7] highlighted four modes of battery degradation: loss of the active material, loss of lithium inventory, stoichiometric drift, and impedance change. Cathode particle cracking triggers many, if not all, degradation modes. Among the most cited culprits for particle cracking in high-nickel-content NMC layered cathodes are

[a] *Imperial College London, Department of Materials and London Centre for Nanotechnology, London, SW7 2AZ, UK.*
E-mail: aigerim.omirkhan@imperial.ac.uk, m.p.ryan@imperial.ac.uk
[b] *The Faraday Institution, Quad One, Harwell Science and Innovation Campus, Didcot, OX11 0RA, UK*

oxygen evolution, surface reconstruction resulting in phase change, and strain build-up during the charging process.[8] The interplay between these mechanisms remains poorly understood. However, the electro-chemo-mechanical nature of cracking is apparent with theories likening it to stress corrosion cracking, which takes places due to the combination of tensile stress and a specific corrosive environment, proposed recently.[9,10] Despite extensive research into the structural instability of NMC811 cathodes, there is a lack of quantitative data describing the evolution of the mechanical properties of cathodes both in their pristine state and upon cycling, and their dependence on the state of charge (SOC) of the battery remains poorly understood.

Polycrystalline NMC811 consists of primary particles assembled into spherical secondary particles with diameters typically between 5 and 15 μm. Fracture occurring in these materials can be classified into intergranular and intragranular. Intergranular cracks appear along the grain boundary between the primary particles, while cracks taking place within primary particles are intragranular. This study probes and observes intergranular cracking mode only. Particle cracking is evidenced more often in polycrystalline cathodes due to a strain mismatch and stress concentration compared to single crystal cathodes.[10] Unlike single crystal particles, where the Li pathway for delithiation and lithiation is shorter due to smaller size of particles, in polycrystalline NMC811 the diffusion pathways are longer, and there is a stress mismatch due to the anisotropy of randomly oriented grains during battery cycling.[11] The strain resulting from the lattice parameter change during cathode delithiation (*i.e.*, charging) at a high state-of-charge (SOC) was suggested to lead to particle cracking during prolonged cycling. The authors reported an anisotropic lattice parameter change, whereby the *c*-lattice parameter initially increased upon charging, followed by a dramatic collapse at 4.2 V *vs.* Li/Li^+. Solid-state nuclear magnetic resonance (NMR) and galvanostatic intermittent titration technique (GITT) data showed hindered diffusion of Li ion mobility at high SOC, leading to Li/vacancy ordering which makes further Li extraction problematic leaving untapped capacity in the cathode material.[12]

The SOC heterogeneity of secondary NMC particles is a known phenomenon.[13] Primary particles in polycrystalline NMC particles are all randomly oriented. This leads to random expansion (*c*-lattice) and contraction (*a*-lattice) during delithiation, creating heterogeneous strain fields. Within a single NMC811 crystal, lithium heterogeneity was particularly strong at the beginning of the charge and at the end of the discharge owing to the varying lithium diffusion coefficients.[14]

Although numerous studies have identified cracking and phase changes as key factors in NMC811 degradation, there is a lack of direct, quantitative analysis on how these factors evolve during electrochemical cycling and impact mechanical stability. To our knowledge, few studies have been carried out to evaluate the local mechanical properties of polycrystalline NMC811 cathodes in the delithiated state at a high SOC. One method of directly assessing the mechanical properties of cathode materials charged to different SOC involves micromechanical testing. A previous study measuring the bulk cathode properties of single crystal NMC811 cathode material indicated shear strength reduction of the cathode in delithiated state.[15] Using large loads for indentation, the results of this study lay important foundation to quantify bulk mechanical properties of the bulk material, although the fracture evolution could not be tracked *in situ*. In another study, polycrystalline NMC111 cathode particles were subjected to flat punch indentation in load-controlled mode inside an argon filled glovebox.[16] The authors showed that the fracture strength decreased dramatically after the first delithiation and lithiation compared with that of the pristine particles. The critical load was inferred from the load–displacement graphs. In a more recent study, the authors have used a conospherical tip to study the fracture strength of NMC811 polycrystalline particles in pristine, electrolyte-soaked and charged states.[17] The authors observed reduced fracture strength upon delithiation of the particles. Critically, this study was performed on NMC811 *vs.* Li metal half-cells. It is known that while useful for isolating cathode behaviour, half cells can be subject to artifacts from Li metal reactivity. Particularly, it has been shown that parasitic reactions products cross over to cathode side and increase the impedance of the cell.[18] Therefore, it is crucial to understand how NMC811 mechanical properties change during cycling in full cell configuration to capture realistic multi-mechanism degradation and reflect the real use case of these cathodes in Li-ion batteries.

It is generally agreed that the stable cathode–electrolyte interphase (CEI) plays an important role in optimizing the battery performance. CEI layer is believed to consist of a mixture of organic and inorganic components, with the latter providing mechanical and chemical stability while allowing for lithium transport.[19,20] It is formed during initial slow charging and discharging of the battery similar to solid electrolyte interphase on anode side, which makes formation steps extremely important for battery stability.[21] To our knowledge, there have been no studies on the effect of formation cycles on the mechanical properties of the NMC811 cathode material. It is equally important to consider the electrolyte composition as it directly influences the CEI. For example, ethylene carbonate (EC) containing electrolytes have been shown to produce non-uniform CEI,[22] which in turn can exacerbate degradation of the electrode. Indeed, NMC811 cathodes cycled in EC containing electrolytes exhibit thicker rock-salt layer as well as increased impedance.[23] While EC is known to accelerate degradation, it remains a widely used component in commercial electrolytes. Therefore, understanding mechanical degradation in baseline EC-containing electrolytes is essential to reflect real-world conditions and guide future improvements.

In our previous study, we demonstrated the use of *in situ* scanning electron microscope (SEM) micromechanical tests to track and identify the fundamental failure modes of pellets synthesised from single- and polycrystalline NMC811.[24] We found that for polycrystalline sintered NMC811 pellets the fracture happened in brittle way only at grain boundaries as opposed to within primary particles. Herein, we propose the use of flat punch compression testing of individual NMC811

polycrystalline secondary particles to quantify the strength of the particles inside the SEM. This method is well established in the literature for measuring the strength of spherical particles and can be accurate even for irregularly shaped particles.[25] Unlike the cono-spherical tip that fractures the sample from the loading point at the surface, the flat punch indentation creates a diametrically symmetrical stress concentration within a particle during loading. By gradually increasing the load in displacement-controlled mode and tracking the fracture evolution with SEM frames, we are able to fully resolve the cracking taking place in individual secondary NMC811 particles. We also performed nanoindentation tests for pristine and delithiated samples to support the observations provided by powder compression tests. This study addresses these critical gaps by employing *in situ* SEM micromechanical testing to quantitatively assess the mechanical degradation of NMC811 cathodes during electrochemical cycling, providing unprecedented insights into the interplay between SOC and evolution of mechanical properties.

In this communication we demonstrate the use of powder compression tests *in situ* SEM to assess the mechanical properties of NMC811 cathodes in the pristine, delithiated, (re)lithiated and aged samples after 50 and 100 cycles cycled in full coin cell configurations in LP50 electrolyte (1 M LiPF6, 1 : 1 weight ratio EC : EMC). We report significant strength reduction upon the very first delithiation charge, followed by a partial recovery of the mechanical strength during discharge, most likely due to reversible anisotropic stain as well as crack closing phenomena previously reported in the literature.[10,26,27] Upon further cycling of the battery, mechanical properties of the NMC811 cathode are seen to gradually degrade. Similar findings are observed through *in situ* nanoindentation measurements carried out to validate the powder compression technique. This methodology can be applied to alternative battery chemistries as a rapid and reliable way to measure the mechanical property as a function of the electrochemical cycling history. It can also be applied as a screening tool to evaluate the effectiveness of coatings, doping, or hierarchical structures designed to mitigate cathode degradation and improve the mechanical stability of cathodes.

Results and discussion

Electrochemical cycling of secondary NMC811 cathode particles results in particle cracking

Polycrystalline NMC811 particles were characterised under different electrochemical states. Fig. 1 shows the SEM micrographs of pristine, delithiated, lithiated and aged polycrystalline NMC811 particles following prolonged cycling. The morphology of the secondary particles in the as-received state is shown in Fig. 1a-2 and in SI1: Fig S2a and b, where the 100–300 nm range primary particles are assembled into spherical secondary particles of 5–15 μm diameter. No cracks were observed in the cross sections of pristine, as-received NMC811 cathode particles (Fig. 1a-1). Following 2 formation cycles at C/20 rate and 1 charge to 4.2 V at C/3 rate, there are no apparent cracks on the top view SEM image (Fig. 1b-2). However, once the cross-section was exposed using broad-beam argon milling, small cracks were observed at the centre of the delithiated particle (Fig. 1b-1). Note that similar result is observed when the cross-sectioning was carried out using either a Ga^+ ion beam or Xe plasma, confirming that the preparation method did not induce cracking of the material (SI1: Fig. S3a and b). There was also a noticeable increase in porosity between the primary particles of NMC811 in the delithiated state, compared to the homogeneity observed in the pristine particles. This can be related to the primary particle inhomogeneity and lattice mismatch at high SOC.[12,28] The origin of this lattice mismatch lies in the formation of rigid rock-salt or spinel layers on the surface of the layered NMC811. During delithiation, the layered structure undergoes *a*/*b* lattice parameter contraction and initial *c*-axis expansion, followed by rapid contraction. On the other hand, the rock-salt structure remains unchanged owing to the absence of Li activity, resulting in a considerable lattice mismatch during delithiation at high SOC. Indeed, TEM characterisation of the NMC811 sample delithiated to 4.2 V *vs.* Li/Li^+ confirms the presence of rock-salt layer, alongside cation-mixed and layered structures (SI1: Fig. S4).

Fig. 1c-1 shows the cross sections of two (re)lithiated NMC811 particles: one with a visible crack at the centre and one without. Study of intragranular cracking in polycrystalline NMC811 showed reversible formation of nanoscale cracks at delithiated state in early cycling.[29] If no contact with electrolyte has occurred, these closed yet resulted in increased lattice spacing. Over time, the surface was irreversibly reduced as evident by evolution of rock-salt layer that was found inside the primary particle. Similarly, initial intergranular cracks (and pores) in secondary particles were shown to close up upon (re)lithiation during discharge as evidenced by operando X-ray computed tomography (XCT).[26] Authors tracked the particles during 10 cycles and showed that cumulative effect of volume expansion and contraction over repeated cycles lead to more damaged particles. It must be noticed that the small cracks similar to one depicted in Fig. 1c-1 can be challenging to track *via* XCT as its size is much smaller than the resolution of the synchrotron technique (<325 nm).

Upon ageing the sample through continuous cycling between 2.5 V and 4.2 V, cracks become visible on the external faces of the particle, suggesting that the internal cracks are now more established on the surface of the particle (Fig. 1d-2). This agrees with the significant cycle-on-cycle capacity reduction seen during electrochemical cycling of the cell in Fig. 1d-3. When cracks are sufficiently wide for the electrolyte ingress, fresh cathode areas are exposed to electrolyte infiltration. The reaction takes place at these sites, resulting in CEI formation, which reduces the amount of active material and increases the cathode impedance. It also creates more surface for cation mixing, rock-salt reconstruction and gas evolution.[23,30] This increases the fatigued phase concentration, which is defined as areas with large mismatch between the layered and epitaxially grown rock-salt layers.[28] Quantifying the strength of NMC811 particles as a function of state of charge and cycling history is an important step in understanding the link between

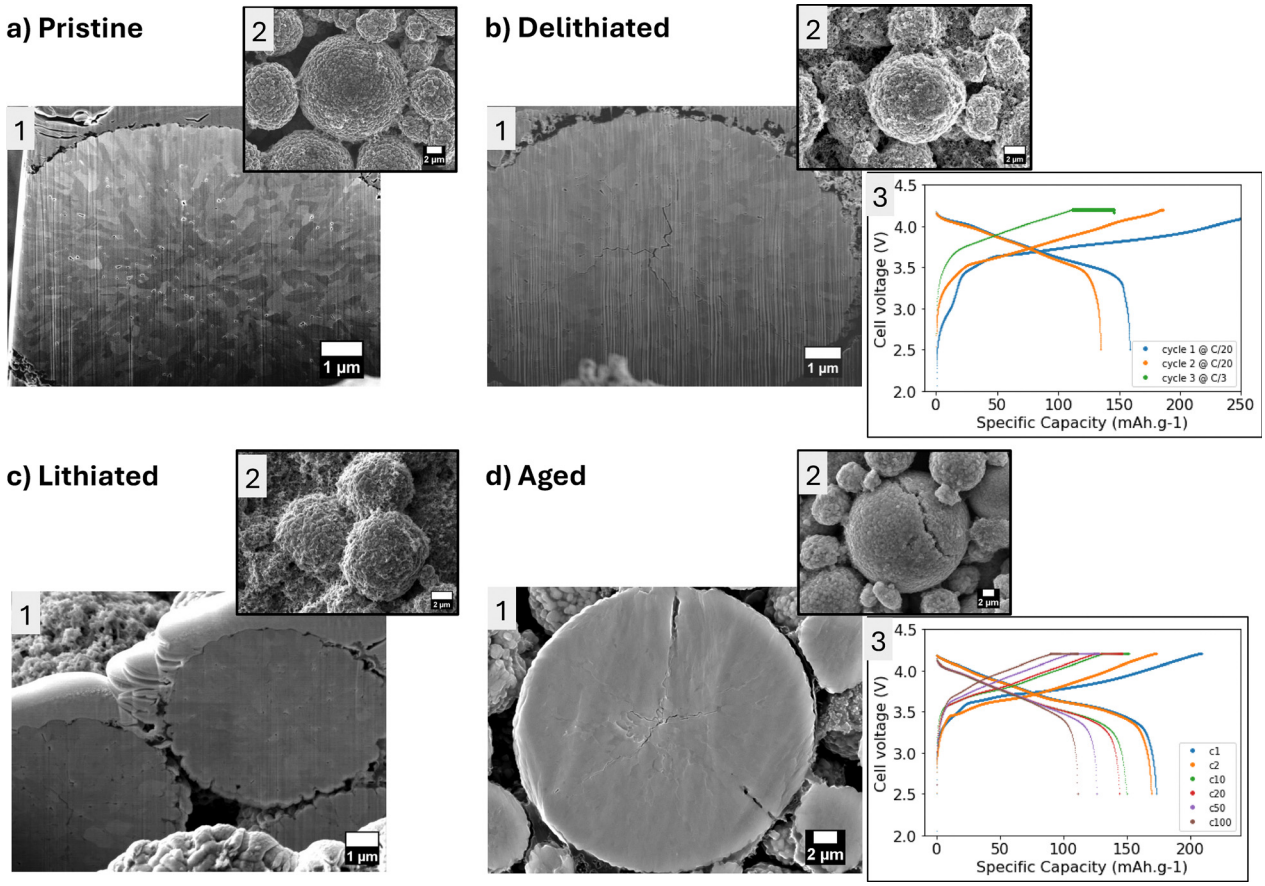

Fig. 1 SEM characterisation and electrochemical cycling of NMC811 cathodes. (a) Cross section of pristine polycrystalline uncalendered NMC811 cathode showing absence of crack at the centre (1). No cracks are visible on the surface of the secondary particles (2); (b) cross section of NMC811 cathode particle in delithiated state showing the presence of the crack at the centre of the particle (1). The cracks were not visible on the surface SEM images (2). The sample was extracted from the full cell configuration cycled with 2 formation cycles at C/20 rate and 1 charging cycle at C/3 rate (3); (c) the cross section of the (re)lithiated samples showing two particles: with (left) and without (crack) in the center (1). No cracks were visible on top SEM images (2); (d) the cross section of aged NMC811 cathode particle (1) in (re)lithiated state showing the cracks at the centre of the particle. Cracks can also be observed on outer surfaces of secondary particles (2). The sample was cycled in a full cell configuration with 2 formation cycles at C/20 rate and 98 cycles at C/3 rate (3).

de(lithiation), ageing and ultimate degradation of cathode materials. It is crucially important to understand whether the apparent reduction of both intragranular and intragranular cracks upon (re)lithiation of cathode reported in the literature[10,26] and herein has any measurable effects on particle mechanical strength. In the next section, we demonstrate that mechanical properties of the NMC811 cathode material are directly dependent on the electrochemical cycling history and state of charge using *in situ* SEM micromechanical testing.

In situ SEM micromechanical testing of polycrystalline NMC811 cathode material

In situ micromechanical testing was used to measure the evolution of mechanical properties as a function of the electrochemical cycling history. In particular, we demonstrate the use of powder compression as a robust method to quantify particle strength, following the methodology originally developed by Hiramatsu and Oka to determine the tensile strength of irregular rock pieces.[25] In this methodology the tensile strength of the particle can be approximated to 0.9 times the critical load divided by the square of the particle diameter, *i.e.* the distance between loading points. This assumes that the fracture takes place due to tensile stress over the centre of the particle. Fig. 2a and b present the SEM images just before and immediately after crack appearance on the pristine, which exists in the lithiated state, NMC811 particle (full videos of particle loading tests can be found in SI2). Similar SEM images are presented in Fig. 2c and d for the delithiated NMC811 particle extracted from a full coin cell charged to 4.2 V at C/20 rate. The fracture of the particles occurred at loads denoted in Fig. 2e as the critical load, F_0. For both pristine (lithiated) and delithiated particles, the crack propagates from the centre of the particle along the grain boundaries between the primary particles. For similar particle sizes, the critical load for delithiated particles $F_{0,d}$ is considerably lower than that of the pristine, lithiated cathode particles $F_{0,p}$. This indicates a reduction in the strength of the particles upon delithiation during the battery charging, even on the first cycle.

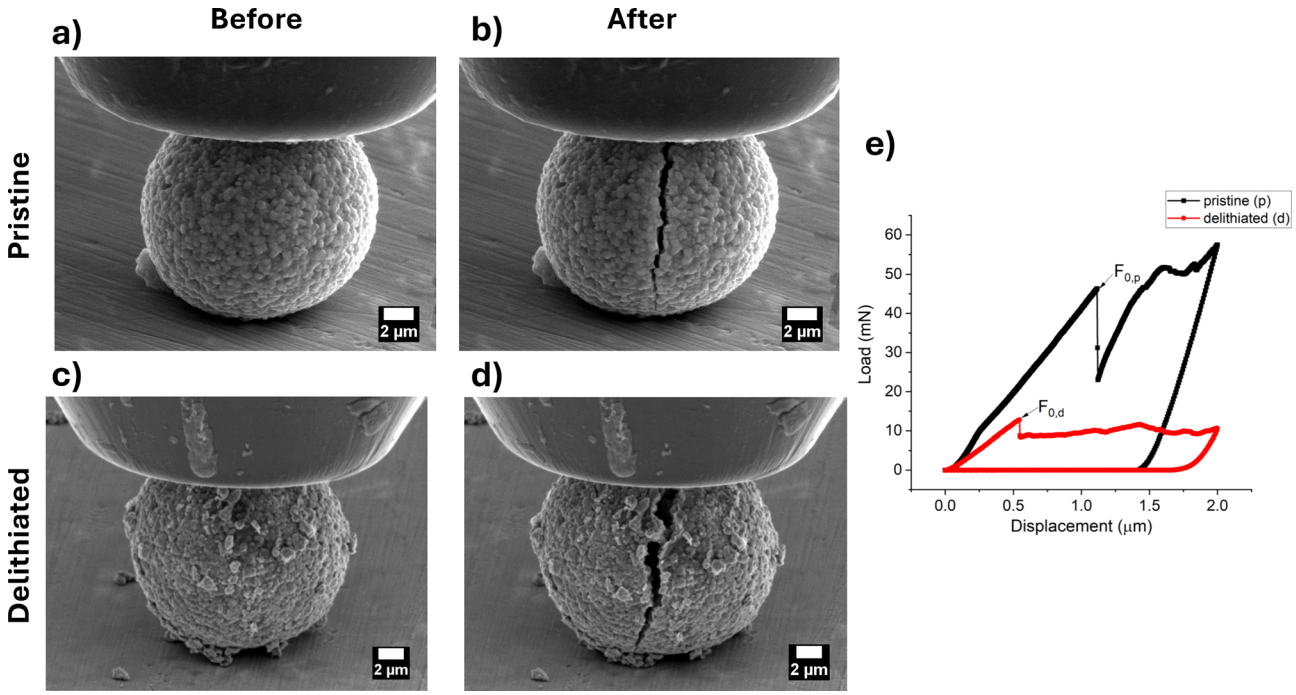

Fig. 2 The SEM images of NMC811 secondary particles before and after intragranular crack appearance in the pristine (a) and (b) and delithiated (c) and (d) states. The corresponding load–displacement curves (e) are presented with the critical loads denoted as $F_{0,p}$ and $F_{0,d}$ for pristine and delithiated particles respectively.

Strength of pristine NMC811 samples. Fig. 3 presents the results averaged from 277 powder compression tests across 25 samples in pristine, delithiated, lithiated states, and aged after 50 and 100 cycles (see SI1, Table S1 for number of particles tested per sample). Broadly, there was no correlation between the particle strength and the diameter of the cycled particles (SI1: Fig. S6). The strength of the particles was calculated using Hiramatsu and Oka equation mentioned earlier. As-received pristine NMC811 cathode samples extracted from cast cathode sheets had strengths of 210 ± 53 MPa and 223 ± 71 MPa for calendered and non-calendered samples respectively. Since these samples were sourced from different suppliers, and given the standard deviation reported, we are unable to confirm if the calendaring process affected the strength of the particles. We have also exposed several particles to air for 2 hours and did not observe statistically significant strength reduction (199 ± 52 MPa). Pristine powder sample had strength of 225 ± 67 MPa and is in good agreement with non-calendered cast electrode sample.

Strength of delithiated NMC811 samples. As mentioned in the previous section, the cross-section SEM images revealed the presence of cracks in the sample charged to 4.2 V at C/20 rate. These particles had the average strength of 16 ± 22 MPa in non-calendered sample, while calendered samples had average strength of 41 ± 26 MPa and 40 ± 16 MPa across two samples, indicating a dramatic decrease in strength during the first delithiation event. Calendering electrodes is known to enhance interfacial contact, which can improve rate capability during cycling.[31] During slow delithiation at C/20, differences in lithium extraction between calendered and uncalendered electrodes may become particularly pronounced. In this context, powder compression can serve as an early indicator of future rate performance, offering insight into how mechanical processing influences electrochemical behaviour.

In situ nanoindentation was used to corroborate single particle powder compression test results. Fig. 4 presents the snapshots taken during nanoindentation test, where the delithiated polycrystalline NMC811 particle cross-section was subject to 3 mN load. The hardness and elastic modulus of the pristine (lithiated) NMC811 particle cross-sections were compared to that of charged (delithiated) NMC811 particles in Table 1. The mechanical properties obtained from nanoindentation are in good agreement with those derived from powder compression, where significant reduction is seen at high SOC. Lithium ions shuttle out of the NMC811 structure during charging, resulting in a significantly weaker structure. As mentioned previously, TEM characterisation of delithiated NMC811 revealed the presence of rock-salt layer alongside layered and cation-mixed phases. This can result in significant anisotropic strain in the material. Fig. 4a and b reveal the presence of intergranular gaps at the boundaries between primary particles in the delithiated NMC811 sample at high SOC, observable as distinct separations along the grain boundaries. This apparent reduction in boundary strength, exacerbated by strain due to phase change, is one of the reasons for the decreased hardness observed in the nanoindentation tests. Voids between the primary particles of NMC811 at delithiated state are commonly occurring phenomena and were observed in TEM analysis (see SI1: Fig. S4a and b) as well as during Atom Probe Tomography (APT) sample preparation (SI1: Fig. S5).

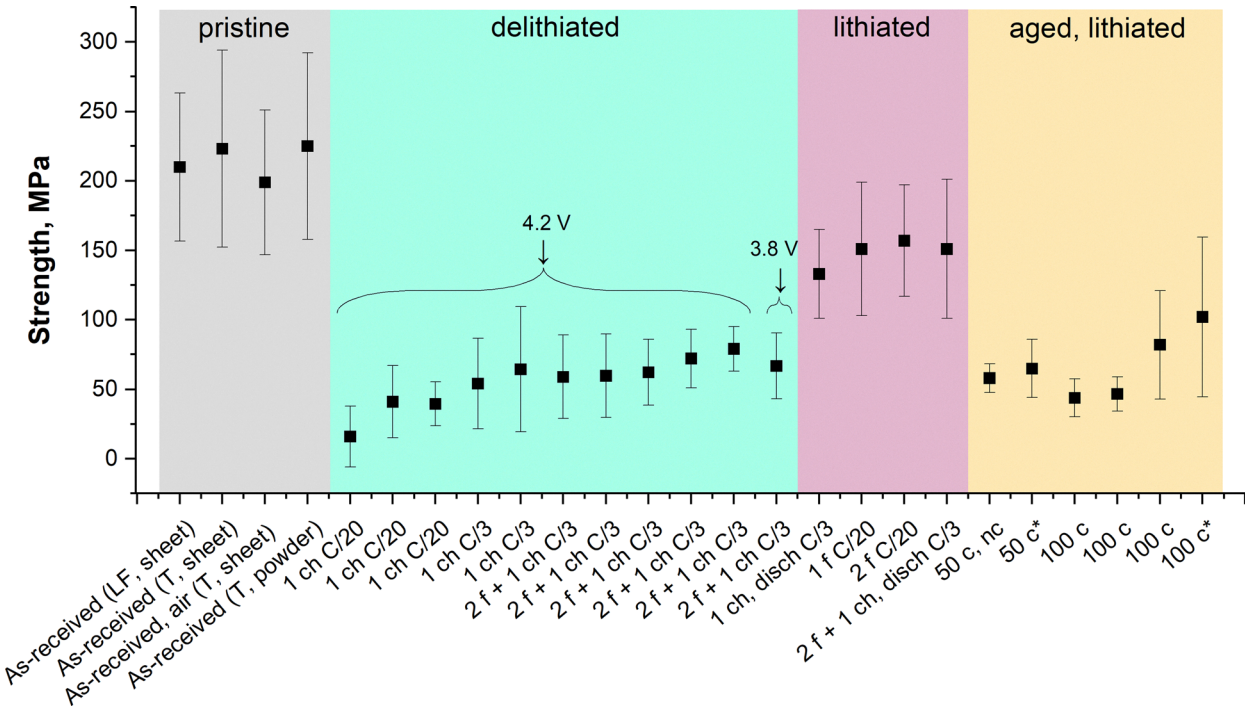

Fig. 3 Average particle strength of polycrystalline NMC811 as a function of electrochemical cycling history, comparing pristine and cycled samples in delithiated, lithiated, and aged states. Error bars represent standard deviation. Pristine particles were either in powder form or extracted from cast sheet electrodes provided by two suppliers: Targray Technology International (non-calendered, T) and Li-FUN Technology (calendered, LF). Cycled particles were obtained from NMC811 *vs.* graphite coin cells cycled in LP50 electrolyte, unless marked with an asterisk (*), indicating NMC811 *vs.* lithium metal cells. Aged samples are in the lithiated state. Electrochemical history is denoted using the following notation: ch – charged; disch – discharged; f – formation cycle; C/3 and C/20 – cycling rates. For example, "2f + 1 ch C/3" indicates 2 formation cycles (at C/20 rate) followed by 1 charge at C/3 rate, resulting in a delithiated cathode state.

It should be noted that powder compression was prioritised over nanoindentation due to its ability to directly probe the mechanical response of individual polycrystalline NMC811 particles without the need for extensive surface preparation, enabling higher throughput characterisation under conditions representative of the native particle morphology.

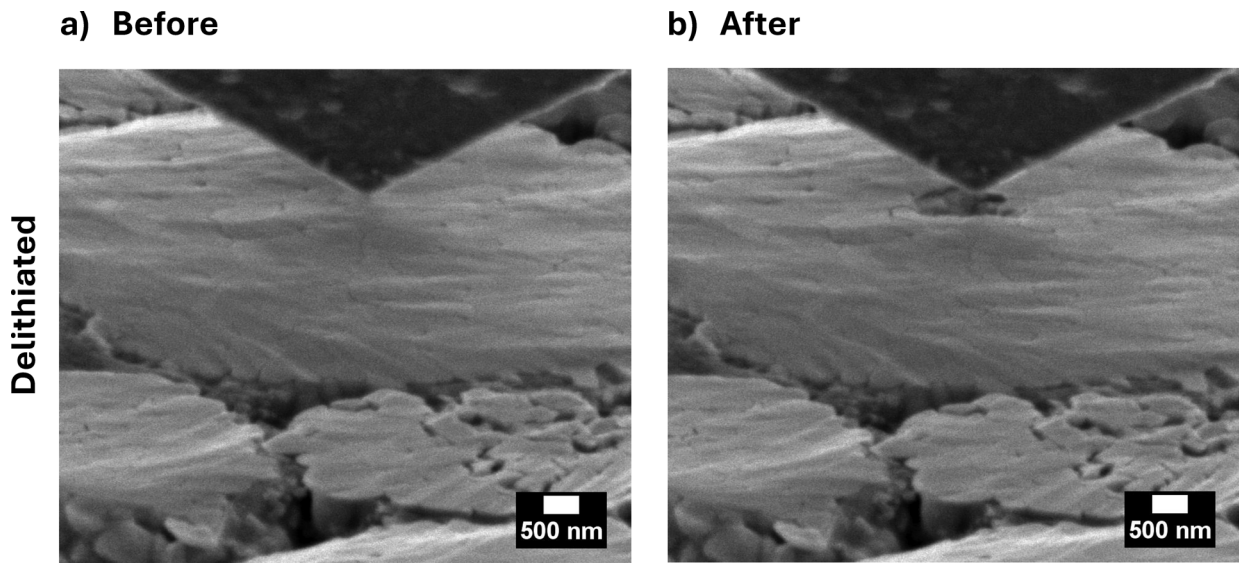

Fig. 4 Snapshots extracted from a real time video recorded during *in situ* nanoindentation testing showing the cross-section of NMC811 sample and the cube corner nanoindenter tip (a) prior to and (b) following the application of a 3 mN load. The sample was charged to 4.2 V *vs.* Li/Li^+ and disassembled in the delithiated state.

Table 1 The hardness and Young modulus of pristine, as-received (lithiated) and delithiated NMC811 samples extracted from *in situ* load–displacement curves

NMC811 state of lithiation	Hardness, GPa	Elastic modulus, GPa
Pristine, lithiated	10.95 ± 3.33	120 ± 22
Delithiated (NMC811 *vs.* Li half-cell)	4.72 ± 0.28	49 ± 4
Delithiated (NMC811 *vs.* C full cell)	3.06 ± 0.30	38 ± 5

Samples delithiated at C/3 rate had higher average strength *vs*. ones delithiated at C/20: with values between 54 ± 33 MPa and 65 ± 45 MPa. This most likely takes place due to overall lower SOC (more lithium in cathode structure) of the battery at C/3 *vs.* C/20 resulting in slightly stronger particles. In the delithiated samples, the average strength of samples with 2 formation cycles was 23 MPa higher than those without formation cycles, highlighting the importance of formation cycles in informing battery degradation among other well-known benefits. Formed samples had average strength values between 59 ± 30 and 79 ± 16 MPa. Note that this is more than 70% reduction of strength seen during the first few cycles in delithiated samples compared with pristine samples.

Strength of lithiated NMC811 samples. Notably, in the samples that were (re)lithiated, *i.e.* charged and discharged at C/20 during 1 formation cycle, we see a partial recovery of mechanical properties to 151 ± 48 MPa. There is an inverse correlation between the state of charge, *i.e.* degree of delithiation, of NMC811 particle and its strength (Fig. 3: see delithiated *vs* lithiated samples). Particles at low SOC have higher strength than particles at high SOC. The partial recovery of mechanical strength of the particles could be attributed to partial intergranular crack closure upon (re)lithiation in early stage cycling as reported in the literature (*operando* XCT studies mentioned in the previous section[26,32]). It is worth mentioning that once the crack forms during delithiation, it does not fully close when (re)lithiated (one would expect the particle strength to revert to original value if crack 'healed'). Nevertheless, we can see that the interparticle grain boundary strength that we probe with *in situ* SEM powder compression is partially regained when lithium ions shuttle back into the NMC811 structure. Recent publication discusses structural changes taking place during NMC811 charge–discharge.[8] Specifically, using *operando* XRD authors reveal a universal mechanism where strain and lattice distortions intensify below a critical lithium content (around 40%). When lithium content in NMC811 lattice went below this critical value, exponential strain and large lattice distortions were measured. In early cycles, the anisotropic strain was measured to be reversible and suggests that initial structural distortions caused by lithium extraction can be recovered upon (re)lithiation. This directly impacts crystalline cracks, which are closely linked to anisotropic strain and lattice distortions. This agrees with our observations, where the strength is partially regained during (re)lithiation. For operating voltages between 2.5–4.2 V authors didn't see any H2 → H3 phase transition (hexagonal with lattice constant $c_{H2} > c_{H3}$), often blamed for capacity fade in nickel-rich layered materials. Similarly, a different study that employed operando XRD and NMR did not see any H2 → H3 at high SOC. They also measured anisotropic lattice expansions, and hypothesised that lead to strain within particles, which can eventually cause particle cracking during long term cycling.[9]

To summarise, the partial strength recovery we measure with *in situ* powder compression is the result of reversible anisotropic strain and lattice distortion. Crucially, our results show that the strength recovery is only partial, suggesting that lithium inhomogeneities already exist in the structure during early cycling. As the lithium inventory is lost during extended cycling, the anisotropy intensifies, resulting in more established cracks that further exacerbate the degradation.

For lithiated samples that have undergone cycling with and without formation cycles, we observed a variation in particle strength values. For example, the particle strength for sample that was cycled once at C/3 rate without formation cycle was 133 ± 32 MPa *vs.* the one with 2 formation cycles at C/20 and 1 cycle at C/3 rate was 151 ± 50 MPa. The strength of particles with just 1 formation cycle at C/20 rate was 151 ± 48 MPa, and 158 ± 31 MPa with two formation cycles at C/20. Slight improvement in particle strength in samples *with* formation cycles at C/20 charging rate as opposed to cycling at C/3 rate indicates that initial slow charging during formation cycles is important in improving the strength of the secondary particles. This may be happening *via* coupled electrochemical and mechanical strengthening through formation of the stable cathode–electrolyte interphase during slow delithiation and lithiation. Further work could concentrate on exploring this concept by exploring the strength evolution of doped, coated electrodes or systems with CEI stabilising electrolyte additives.

Strength of aged NMC811 samples. Finally, we can see in Fig. 3 that aging NMC811 material *via* extended cycling results in further reduction of the particle strength compared to as-received and lithiated samples. Across 6 aged samples, the particle strength after 50 cycles was 58 ± 10 MPa (full cell) and 65 ± 21 MPa (half-cell); while the variation after 100 cycles was quite prominent with average strength values between 44 ± 14 MPa and 82 ± 39 MPa measured for full cells, and 102 ± 58 MPa for half-cell configurations. Interestingly, this gradual reduction during aging is recorded both in high-capacity cells and cells with average performance (SI1: Fig. S8) as cycle-on-cycle capacity reduction is measured in all aged samples. This is likely caused by formation of permanent cracks (*i.e.* cracks that reach the surface of the particle and do not reduce in size on cycling), through layered structure transformation into the spinel and rock-salt structures, increasing lattice mismatch between these structures. Indeed, it was reported that prolonged cycling in polycrystalline NMC811 particles is associated with atomic-level transformations including rock-salt layer formation on crack surfaces, transition metal dissolution consistent with rock-salt layer, as well as strain and lattice distortions using scanning transmission electron microscopy (STEM) and electron energy loss spectroscopy (EELS).[29] Another study presented the TEM results of aged NMC811 samples after 100 cycles, where electrochemically inactive rock-salt layer

was found on the surface of the particles.[6] Although it was proposed in previous studies that capacity fade may be linked to particle cracking, here we directly measure the evolution of mechanical properties as function of their state of charge and cycling history in full cell configuration. These results are important because we demonstrate that even under 'normal' cycling conditions of up to 4.2 V polycrystalline NMC811 particles lose their mechanical stability as evidenced by reduced particle strength in aged samples.

With the current trend towards even higher nickel cathode chemistries, where cracking is a commonly encountered issue,[33] it is crucial to understand how cycling and state of charge affects the particle strength. Our results demostrate that powder compression *in situ* SEM enables rapid quantification of these effects. This approach allows us to quantify the effect of SOC and the electrochemical cycling history on mechanical stability of these particles. We also report a mechanical property improvement in samples that underwent 2 full formation cycles as opposed to the ones without formation cycles, thus supporting earlier suggestions that battery degradation can be electrochemical-chemo-mechanical in nature. This method can be applied to evaluate other cathode chemistries (*e.g.* Na-ion cathodes such as sodium vanadium phosphate[34]) where the particle integrity plays an important role in battery performance. There is a potential to use this technique as a screening tool to evaluate the efficiency of NMC811 degradation mitigation strategies including surface treatment methods such coatings and doping, or hierarchical structures such as core–shell. The method can also be used to validate the development of novel electrolyte blends and additives that suppress the capacity loss seen in NMC811. For example, development of EC-free electrolytes as it is widely known that EC can promote degradation of NMC811 cathodes through lattice oxygen loss, surface reconstruction and surface impedance growth.[23,30,35]

Conclusions

The micromechanical testing conducted *in situ* SEM in this study provides direct observation and measurement of the mechanical strength of the polycrystalline NMC811 cathode in pristine, cycled, and charged states. At high states of charge, NMC811 undergoes severe mechanical strength reduction due to crack formation because of anisotropic lattice parameter changes and strain mismatches in the polycrystalline material. While some strength recovery occurs upon discharge, most likely related to crack size decrease and reversible anisotropic strain,[26,27] continuous cycling results in considerable irreversible mechanical degradation, likely due to crack propagation. This in turn will result in active material loss, fresh surface reaction with electrolyte producing gases, and rock-salt layer formation contributing to the impedance growth and material degradation.[4,7,12,30] This work offers valuable insights in form of quantification of the mechanical strength as a function of the electrochemical cycling history in realistic full cell battery configurations with EC containing electrolyte. The study is particularly relevant as electric vehicle battery chemistries are trending towards higher nickel content electrodes, where rock-salt layer forms upon cycling to high voltages therefore increasing the lattice anisotropy. Findings contribute to our understanding of why and how battery cathode materials degrade, which is crucial for improving the performance and longevity of high-nickel content lithium-ion batteries. The powder compression testing *in situ* SEM can be applied to other materials chemistries and used as a reliable and quick method to quantify the mechanical stability of spherical cathode particles, evaluate the novel electrolyte formulations and other mitigation strategies such as surface and lattice modifications.

Author contributions

A. O. conceptualisation, data curation, formal analysis, investigation, methodology, validation, visualisation, writing original draft, writing – review & editing; O. G. D. methodology, investigation, writing – review & editing; S. W. methodology, writing – review & editing; M. P. R. conceptualisation, funding acquisition, supervision, writing – review & editing; I. E. L. S funding acquisition, writing – review & editing; F. G. resources, methodology, writing – review & editing.

Conflicts of interest

There are no conflicts to declare.

Data availability

The data supporting this study are available in the article and its supplementary information (SI). Supplementary information: SI1 and SI2. See DOI: **https://doi.org/10.1039/d5ee00976f**.

Acknowledgements

A. O., I. E. L. S. and M. P. R. acknowledge Faraday Institution Degradation Project FIRG001, FIRG024 and INFUSE: Interface with the Future – Underpinning Science to Support the Energy transition EPSRC Prosperity Partnership EP/V038044/1 for support. O. G. D., S. W. and F. G. would like to acknowledge the EPSRC Future Manufacturing Hub in Manufacture using Advanced Powder Processes, EP/P006566/1. S. W. acknowledges Imperial College Research Fellowship. M. P. R. acknowledges support from the Armourers and Brasiers Company.

Notes and references

1 W. Liu, P. Oh, X. Liu, M. J. Lee, W. Cho, S. Chae, Y. Kim and J. Cho, *Angew. Chem., Int. Ed.*, 2015, **54**, 4440–4457.
2 R. Jung, M. Metzger, F. Maglia, C. Stinner and H. A. Gasteiger, *J. Electrochem. Soc.*, 2017, **164**, A1361–A1377.
3 H. J. Noh, S. Youn, C. S. Yoon and Y. K. Sun, *J. Power Sources*, 2013, **233**, 121–130.

4 W. M. Dose, J. K. Morzy, A. Mahadevegowda, C. Ducati, C. P. Grey and M. F. L. De Volder, *J. Mater. Chem. A*, 2021, **9**, 23582–23596.
5 R. Xu, H. Sun, L. S. de Vasconcelos and K. Zhao, *J. Electrochem. Soc.*, 2017, **164**, A3333–A3341.
6 H. H. Ryu, K. J. Park, C. S. Yoon and Y. K. Sun, *Chem. Mater.*, 2018, **30**, 1155–1163.
7 J. S. Edge, S. O'Kane, R. Prosser, N. D. Kirkaldy, A. N. Patel, A. Hales, A. Ghosh, W. Ai, J. Chen, J. Yang, S. Li, M. C. Pang, L. Bravo Diaz, A. Tomaszewska, M. W. Marzook, K. N. Radhakrishnan, H. Wang, Y. Patel, B. Wu and G. J. Offer, *Phys. Chem. Chem. Phys.*, 2021, **23**, 8200–8221.
8 P. Li, Y. Zhao, Y. Shen and S.-H. Bo, *JPhys Energy*, 2020, **2**, 022002.
9 W. Wei, Z. Ding, C. Chen, C. Yang, B. Han, L. Xiao, C. Liang, P. Gao and K. Cho, *Acta Mater.*, 2021, **212**, 116914.
10 Y. Dong and J. Li, *Chem. Rev.*, 2023, **123**, 811–833.
11 J. C. Stallard, L. Wheatcroft, S. G. Booth, R. Boston, S. A. Corr, M. F. L. De Volder, B. J. Inkson and N. A. Fleck, *Joule*, 2022, **6**, 984–1007.
12 K. Märker, P. J. Reeves, C. Xu, K. J. Griffith and C. P. Grey, *Chem. Mater.*, 2019, **31**, 2545–2554.
13 W. E. Gent, Y. Li, S. Ahn, J. Lim, Y. Liu, A. M. Wise, C. B. Gopal, D. N. Mueller, R. Davis, J. N. Weker, J.-H. Park, S.-K. Doo and W. C. Chueh, *Adv. Mater.*, 2016, **28**, 6631–6638.
14 C. Xu, A. J. Merryweather, S. S. Pandurangi, Z. Lun, D. S. Hall, V. S. Deshpande, N. A. Fleck, C. Schnedermann, A. Rao and C. P. Grey, *Joule*, 2022, **6**, 2535–2546.
15 J. C. Stallard, S. Vema, D. S. Hall, A. R. Dennis, M. E. Penrod, C. P. Grey, V. S. Deshpande and N. A. Fleck, *J. Electrochem. Soc.*, 2022, **169**, 40511.
16 D. Dang, Y. Wang and Y.-T. Cheng, *J. Electrochem. Soc.*, 2019, **166**, A2749–A2751.
17 L. Wheatcroft, A. Bird, J. C. Stallard, R. L. Mitchell, S. G. Booth, A. J. Nedoma, M. F. L. De Volder, S. A. Cussen, N. A. Fleck and B. J. Inkson, *Batteries Supercaps*, 2023, **6**, e202300032.
18 R. C. McNulty, E. Hampson, L. N. Cutler, C. P. Grey, W. M. Dose and L. R. Johnson, *J. Mater. Chem. A*, 2023, **11**, 18302–18312.
19 N. Zhang, B. Wang, F. Jin, Y. Chen, Y. Jiang, C. Bao, J. Tian, J. Wang, R. Xu, Y. Li, Q. Lv, H. Ren, D. Wang, H. Liu, S. Dou and X. Hong, *Cell Rep. Phys. Sci.*, 2022, **3**, 101197.
20 Q. Zhang, J. Pan, P. Lu, Z. Liu, M. W. Verbrugge, B. W. Sheldon, Y.-T. Cheng, Y. Qi and X. Xiao, *Nano Lett.*, 2016, **16**, 2011–2016.
21 F. Schomburg, B. Heidrich, S. Wennemar, R. Drees, T. Roth, M. Kurrat, H. Heimes, A. Jossen, M. Winter, J. Y. Cheong and F. Röder, *Energy Environ. Sci.*, 2024, **17**, 2686–2733.
22 J. Alvarado, M. A. Schroeder, M. Zhang, O. Borodin, E. Gobrogge, M. Olguin, M. S. Ding, M. Gobet, S. Greenbaum, Y. S. Meng and K. Xu, *Mater. Today*, 2018, **21**, 341–353.
23 W. M. Dose, I. Temprano, J. P. Allen, E. Björklund, C. A. O'Keefe, W. Li, B. L. Mehdi, R. S. Weatherup, M. F. L. De Volder and C. P. Grey, *ACS Appl. Mater. Interfaces*, 2022, **14**, 13206–13222.
24 S. Wang, Z. Shen, A. Omirkhan, O. Gavalda-Diaz, M. P. Ryan and F. Giuliani, *J. Eur. Ceram. Soc.*, 2023, **43**, 7553–7560.
25 Y. Hiramatsu and Y. Oka, *Int. J. Rock Mech. Min. Sci.*, 1966, **3**, 89–99.
26 H. C. W. Parks, M. P. Jones, A. Wade, A. V. Llewellyn, C. Tan, H. T. Reid, R. Ziesche, T. M. M. Heenan, S. Marathe, C. Rau, P. R. Shearing and R. Jervis, *EES Batter.*, 2025, **1**, 482–494.
27 T. Jousseaume, J. F. Colin, M. Chandesris, S. Lyonnard and S. Tardif, *Energy Environ. Sci.*, 2024, **17**, 2753–2764.
28 C. Xu, K. Märker, J. Lee, A. Mahadevegowda, P. J. Reeves, S. J. Day, M. F. Groh, S. P. Emge, C. Ducati, B. Layla Mehdi, C. C. Tang and C. P. Grey, *Nat. Mater.*, 2021, **20**, 84–92.
29 J. K. Morzy, W. M. Dose, P. E. Vullum, M. C. Lai, A. Mahadevegowda, M. F. L. De Volder and C. Ducati, *ACS Appl. Energy Mater.*, 2024, **7**, 3945–3956.
30 D. B. Thornton, B. J. V. Davies, S. B. Scott, A. Aguadero, M. P. Ryan and I. E. L. Stephens, *Angew. Chem., Int. Ed.*, 2024, **63**, e202315357.
31 K. Raju, L. Wheatcroft, M. C. Lai, A. Mahadevegowda, L. F. J. Piper, C. Ducati, B. J. Inkson and M. De Volder, *J. Electrochem. Soc.*, 2024, **171**, 080519.
32 H. C. W. Parks, A. M. Boyce, A. Wade, T. M. M. Heenan, C. Tan, E. Martínez-Pañeda, P. R. Shearing, D. J. L. Brett and R. Jervis, *J. Mater. Chem. A*, 2023, **11**, 21322–21332.
33 L. An, J. E. N. Swallow, P. Cong, R. Zhang, A. D. Poletayev, E. Björklund, P. N. Didwal, M. W. Fraser, L. A. H. Jones, C. M. E. Phelan, N. Ramesh, G. Harris, C. J. Sahle, P. Ferrer, D. C. Grinter, P. Bencok, S. Hayama, M. S. Islam, R. House, P. D. Nellist, R. J. Green, R. J. Nicholls and R. S. Weatherup, *Energy Environ. Sci.*, 2024, **17**, 8379–8391.
34 H. Kashif Razzaq, C.-C. Yang, M. Norhaffis Mustafa, A. Numan and M. Khalid, *Prog. Mater. Sci.*, 2025, **151**, 101424.
35 Y. Zhang, Y. Katayama, R. Tatara, L. Giordano, Y. Yu, D. Fraggedakis, J. G. Sun, F. Maglia, R. Jung, M. Z. Bazant and Y. Shao-Horn, *Energy Environ. Sci.*, 2020, **13**, 183–199.

